Communications in Nonlinear Science and Numerical Simulation 125 (2023) 107407

Contents lists available at ScienceDirect

Communications in Nonlinear Science and Numerical Simulation

journal homepage: www.elsevier.com/locate/cnsns

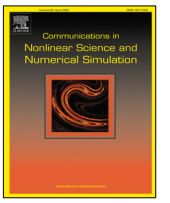

Research paper

Dynamical analysis and reachable set estimation of T-S fuzzy system with permanent magnet synchronous motor

R. Vadivel [a,1], Zeric Tabekoueng Njitacke [b,1], Lakshmanan Shanmugam [c,1], P. Hammachukiattikul [a,1], Nallappan Gunasekaran [d,*,1]

[a] Department of Mathematics, Faculty of Science and Technology, Phuket Rajabhat University, Phuket 83000, Thailand
[b] Department of Electrical and Electronic Engineering, College of Technology (COT), University of Buea, P.O. Box 63, Buea, Cameroon
[c] Division of Mathematics, Vellore Institute of Technology, Chennai 600127, Tamil Nadu, India
[d] Eastern Michigan Joint College of Engineering, Beibu Gulf University, Qinzhou 535011, China

ARTICLE INFO

Article history:
Received 15 January 2023
Received in revised form 5 May 2023
Accepted 27 June 2023
Available online 4 July 2023

Keywords:
Lyapunov–Krasovskii functional
Sampled-data control
T-S fuzzy
PMSM
Reachable set

ABSTRACT

In this study, we will present the dynamical analysis for permanent magnet synchronous motors (PMSM). Our goal is to identify an ellipsoid that contains the state trajectory of the system in as small a form as possible in the presence of control. First, we designed the non-fragile sampled-data fuzzy controller (NFSDFC) for the PMSM model. Second, the Lyapunov-Krasovskii functional (LKF) strategy, novel integral inequality mechanisms, and certain sufficient conditions are determined, which ensure an ellipsoidal bound of reachable sets for the closed-loop of a system with input constraints derived in terms of linear matrix inequalities (LMIs). Meanwhile, under the larger sampling interval, the corresponding sampled-data controller gains are designed. Finally, numerical examples are given to validate the derived theoretical results.

1. Introduction

Over the past few years, a lot of research activities have been devoted to the study of a variety of electric motors. Some of these motors are hybrid step motor drives [1], induction motor drive [2], permanent magnet synchronous motor (PMSM) drive [3,4], voltage and current mode direct current motor drives [5], switched resistance motor drive [6], synchronous reluctance motor drive [7], and brushless direct current motor (BLDCM) drive [8]. Among the most studied motors, there is one called the permanent magnet synchronous motor (PMSM) [9]. Because of their simple form, high efficiency, high power density, and low production cost, the PMSM is extensively utilized in industrial applications such as motor drives, various servo systems, and household appliances. Because of its nonlinear mathematical model, this motor is able to exhibit very rich and complex dynamics, among which is the well-known phenomenon of chaos. Therefore, a huge amount of research effort has been devoted to the study and control of that phenomenon in the PMSM. In fact, in [3], a deep investigation of the bifurcation as chaos for a wide range of parameters has been addressed in a PMSM model with a smooth air gap. The effect of the smooth and the non-smooth air gap has been investigated on the behavior of the studied motor in [9]. In that work, the analysis of the stability of the equilibrium point revealed pitchfork and Hopf bifurcations. More interestingly, numerical simulations highlighted phenomena such as period-doubling bifurcation, cyclic

* Corresponding author.
E-mail addresses: vadivelsr@yahoo.com (R. Vadivel), lakshm85@gmail.com (L. Shanmugam), gunasmaths@gmail.com (N. Gunasekaran).

[1] All authors contributed equally and significantly to the writing of this article and typed, read, and approved the final manuscript.

https://doi.org/10.1016/j.cnsns.2023.107407
1007-5704/

fold bifurcation, single-scroll, and double-scroll chaotic attractors. In [10], the authors introduced a fractional model of the PMSM and followed the bifurcation analysis of that model, which revealed phenomena such as bursting and hidden oscillations. The dynamics of a simplified model of the PMSM have been addressed in [11]. Furthermore, the authors used a simple controller to suppress chaos in the model considered. Additionally, they presented a simple way to synchronize two identical models, and the results have been validated based on an electronic model of the considered motor. Hidden dynamics and multistability of the PMSM have been addressed in [12]. The findings of the authors have been validated on the basis of both theoretical and numerical approaches.

Furthermore, analyzing and understanding nonlinear models using present mathematical methods is substantially more difficult owing to their variations with regard to nonlinearities. As a result, the Takagi–Sugeno (TS) method is used in the literature to illustrate the nonlinearity that can occur with respect to the IF-THEN rules for linear submodels based on fuzzy membership-based rules and has been thoroughly investigated by various scientists over the last several decades [13–17]. For example, adaptive fractional fuzzy integral sliding mode control for the PMSM model has been analyzed in [18]. In [19], we discuss non-fragile distributed filtering for fuzzy T-S systems in sensor networks. Authors in [20], researched quantized sampled-data control for extended dissipative analysis of the T-S fuzzy system. Recently, the Lyapunov-Krasovkii functional (LKF) combined with LMI has become a popular approach for stability analysis and stabilization of the system. Less conservative stability criteria and the controller can be developed by constructing a suitable LKF with more system information [15–17]. Therefore, designing a suitable controller is crucial because studying the PMSM model with input disturbances is a very worthwhile subject.

Numerous control methods, including adaptive control, finite-time H_∞ control, proportional integral derivative control, sliding mode control, and others have been utilized to study the stability behavior of the PMSM model in light of the outstanding results obtained with the T-S fuzzy model. The sampled-data control (SDC), on the other hand, runs continuously while sampling discrete-time signals at certain instants in time. Therefore, continuous and discrete-time signals are both used in digital control systems, which are hybrid systems [15–17,21–24]. SDC provides simple and dependable control in many real-world plants with minor disturbances because it can be easily adjusted to achieve the desired performance. It is utilized in the robust control of many PMSM systems since it also ensures performance and stability, even in the face of uncertainty. Therefore appropriate SDC has been very compatible with PMSM. Several extensive and profitable results have been made about the SDC system [25–29]. On the other hand, a reachable set of dynamic systems is the set that bounds all system state trajectories in the presence of external disturbances. Reachable set estimation (RSE) is a significant issue not only in robust control theory but also in practice, where secured operations are executed through controllers to mitigate insecure regions [30,31]. These characteristics led a few researchers to recently acknowledge the control problems in RSE. Numerous outstanding theoretical results on RSE [32–34] have been developed in recent years. To name a few, [32]. suggested a solution to the RSE and aperiodic sampled-data controller design problems for Markovian jump systems. In [33], the problem of RSE for T-S fuzzy systems against unknown output delays with application to tracking control of AUVs was presented. RSE and controller design for discrete-time singularly perturbed systems with time-varying delays were explored by the authors in [35]. It should be noted that the RSE synthesis and PMSM model-based T-S fuzzy method with non-fragile sampled-data control (NFSDC) have received relatively little attention up to this point.

Inspired by the above facts, the stabilization PMSM model is examined in this study via NFSDC. The principle contribution of the study is summarized as follows:

- The proposed PMSM system was established by considering the influence of the T-S fuzzy approach and has been enforced in approximating the nonlinearities into linear models.
- Furthermore, NFSDC has been introduced in the intended PMSM and can be fully suppressed or driven into a predictable and adjustable bound.
- Utilizing a novel integral inequality and several new suitable conditions, suitable LKF are built for the stability analysis of the proposed system model, and an acceptable RSE synthesis technique is derived to take PMSM into consideration in terms of linear matrix inequalities (LMIs).
- In order to demonstrate the effectiveness and applicability of the given theories, numerical simulations and comparison results are suggested as a final step.

Notations. The issue formulation and primary outcome notations will now be defined. A n-dimensional real matrix is represented by $\mathbb{R}^{n\times m}$ and a n-dimensional Euclidean space by $\mathbb{R}^n$. The identity matrix with the necessary dimensions is denoted by I. It indicates that P is a symmetric, semi-positive-definite matrix (respectively, positive definite matrix) when it is represented as $P \geq 0$ (or $P > 0$). Use M^T and M^{-1} to represent the transpose and inverse of M, respectively. In symmetrical places, the sign $*$ denotes the transposed element. Additionally, $Sym\{X\}$ is defined as $Sym\{X\} = X^T + X$. The symbols diag is used to indicate a block-diagonal matrix. $\|\cdot\|$ stands for the spectral norm for matrices and the Euclidean norm for vector space.

2. Presentation of the PMSM

2.1. Model description

The mathematical expression of the PMSM can be provided based on the d-q axis [3] as presented in (1)

$$\begin{cases} \frac{di_d}{dt} = \left(u_d - R_1 i_d + \omega L_q i_q\right)/L_d \\ \frac{di_q}{dt} = \left(u_q - R_1 i_q - \omega L_d i_d + \omega \psi_r\right)/L_q \\ \frac{d\omega}{dt} = \left[n_p \psi_r i_q + n_p \left(L_d - L_q\right) i_d i_q - T_L - \beta\omega\right]/J \end{cases} \tag{1}$$

where the motor's currents and angular frequency are denoted by i_d, i_q, and ω, respectively. The direct and quadrature-axis stator voltage components are denoted by u_d and u_q, the polar moment of inertia is denoted by J, and the external torque is denoted by T_L. The viscous damping coefficient is denoted by β, the stator winding resistance is denoted by R_1, L_d and L_q have respectively stated the direct and quadrature-axis stator inductors, ψ_r the permanent magnet flux and the number of pole-pairs. By applying the variable change $x = \zeta x_i$, and the time change $\tau = \zeta t$, here $x = \begin{bmatrix} i_d & i_q & \omega \end{bmatrix}^\top$, $x_i = \begin{bmatrix} x_1 & x_2 & x_3 \end{bmatrix}^\top$, $\zeta = \begin{bmatrix} \zeta_d & 0 & 0 \\ 0 & \zeta_q & 0 \\ 0 & 0 & \zeta_\omega \end{bmatrix} = \begin{bmatrix} bk & 0 & 0 \\ 0 & k & 0 \\ 0 & 0 & 1/\tau \end{bmatrix}$.

With $b = \frac{L_q}{L_d}$, $k = \frac{\beta}{n_p \tau \psi_r}$ and $\zeta = \frac{L_q}{R_1}$ we obtain a system of equations in a dimensionless form as:

$$\begin{cases} \frac{dx_1}{dt} = -bx_1 + x_2 x_3 + v_1 \\ \frac{dx_2}{dt} = -x_2 - x_1 x_3 + \gamma x_3 + v_2 \\ \frac{dx_3}{dt} = \sigma\left(x_2 - x_3\right) + \varepsilon x_1 x_2 - v_3. \end{cases} \tag{2}$$

Where $\gamma = \frac{n_p \psi_r^2}{R_1 \beta}$, $\sigma = \frac{L_q \beta}{R_1 J}$, $\varepsilon = \frac{L_q \beta^2 (L_d - L_q)}{L_d J n_p \psi_r^2}$, $v_1 = \frac{n_p \psi_r L_q}{\beta R_1^2} u_d$, $v_2 = \frac{n_p \psi_r L_q}{\beta R_1^2} u_q$, and $v_3 = \frac{L_q^2 T_L}{R_1^2 J}$. The parameters of the PMSM studied in this work are given as: $n_p = 1$, $\psi_r = 1.8$ Nm/A, $R_1 = 0.9\Omega$, $\beta = 0.0162 N/rad/s$, $L_q = 11mH$, $L_d = 15mH$, $J = 4.7 \times 10^{-3} Kgm^2$.

To address the dynamics of this PMSM two assumptions are made: $L_q \neq L_d$, and $u_d = u_q = T_L = 0$.

Then the previous mathematical model Eq. (2) becomes.

$$\begin{cases} \frac{dx_1}{dt} = -bx_1 + x_2 x_3 \\ \frac{dx_2}{dt} = -x_2 - x_1 x_3 + \gamma x_3 \\ \frac{dx_3}{dt} = \sigma\left(x_2 - x_3\right) + \varepsilon x_1 x_2. \end{cases} \tag{3}$$

Using the parameters of the motor, the dimensionless parameters are given as:

$b = 0.733$, $\gamma = 222.222$, $\sigma = 42.127$, $\varepsilon = 0.0505$.

2.2. Dissipation property and stability of the model

The dissipation property of the considered PMSM can be evaluated after the estimation of the volume contraction rate of the considered machine as provided by Eq. (4).

That contraction rate enables us to have an idea of the nature of the behavior generated by the considered machine model. In that way, three types of behaviors can be identified, among which, the dissipative one with $divV < 0$, the conservative one with $divV = 0$, and the repelled one with $divV > 0$.

$$divV = \begin{pmatrix} \frac{\partial}{\partial x_1} \\ \frac{\partial}{\partial x_2} \\ \frac{\partial}{\partial x_3} \end{pmatrix} \cdot \begin{pmatrix} -bx_1 + x_2 x_3 \\ -x_2 - x_1 x_3 + \gamma x_3 \\ \sigma\left(x_2 - x_3\right) + \varepsilon x_1 x_2 \end{pmatrix}. \tag{4}$$

Which gives

$$divV = -b - 1 - \sigma. \tag{5}$$

From Eq. (5), it is obvious that the volume contraction rate of the PMSM depends on the value of some key parameters of the motor. Therefore, the PMSM model will be dissipative if and only if $-b - 1 - \sigma < 0$. Since all the parameters of the dimensionless model of the PMSM are positive, the volume contraction will be negative. Consequently, the considered model is dissipative. The Jacobian matrix of the considered model is given as :

$$J_M = \begin{bmatrix} -b & \bar{x}_3 & \bar{x}_2 \\ -\bar{x}_3 & -1 & \gamma - \bar{x}_1 \\ \varepsilon \bar{x}_2 & \varepsilon \bar{x}_1 + \sigma & -\sigma \end{bmatrix}. \tag{6}$$

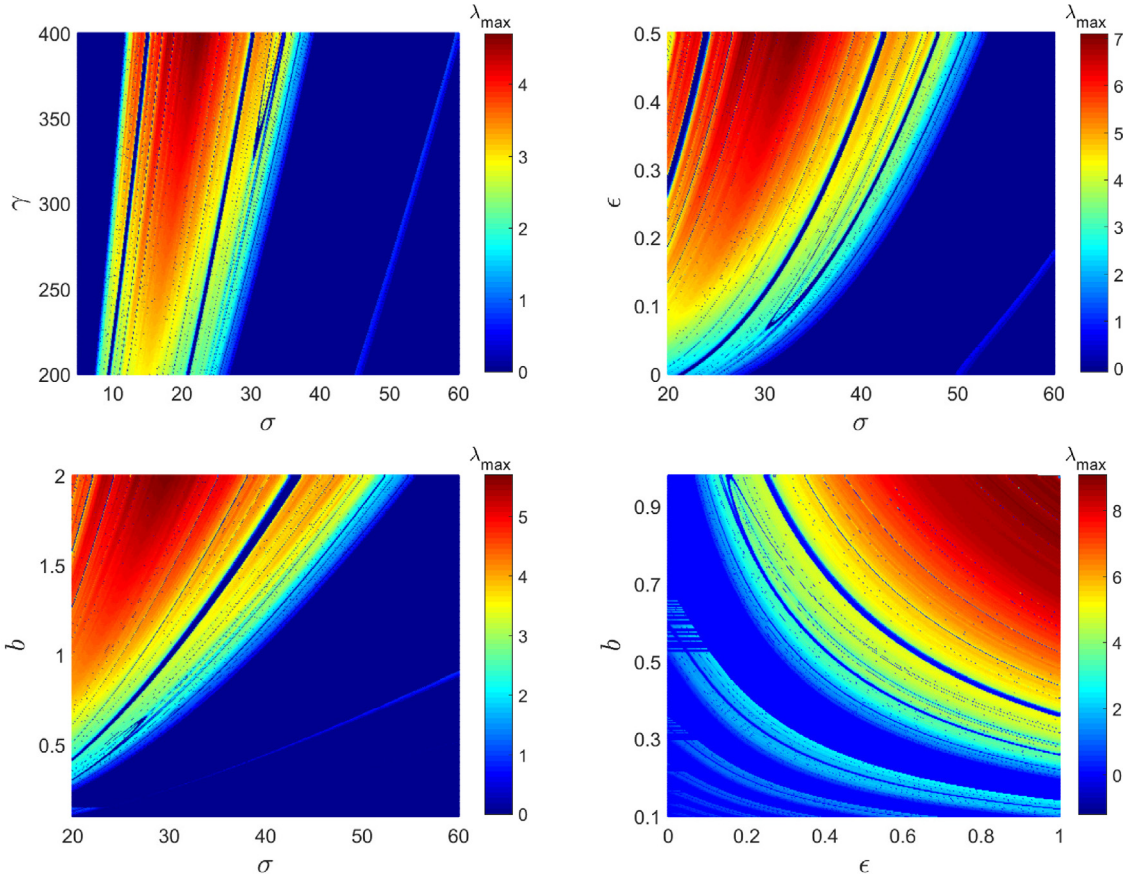

Fig. 1. Two-parameter diagrams showing the general behavior of the considered PMSM with no smooth air gap. The plane (σ, γ) for $b = 0.733, \epsilon = 0.0505$, the plane (σ, ϵ) for $b = 0.733, \gamma = 300$, the plane (σ, b) for $\gamma = 300, \epsilon = 0.0505$ and the plane (ϵ, b) for $\gamma = 300, \sigma = 40$. These diagrams are obtained with the initial conditions (0.1744, 0., 0.221).

Where $(\bar{x}_1, \bar{x}_2, \bar{x}_3)$ are the equilibrium points of the PMSM the characteristic equation around the trivial equilibrium point E_0 (0, 0, 0) is given by :

$$P(\lambda) = \lambda^3 + (\sigma + 1 + b)\lambda^2 + (b\sigma - \gamma\sigma + b + \sigma)\lambda - b\gamma\sigma + \sigma b = 0. \tag{7}$$

From the last coefficient of the characteristic equation, it is obvious that the considered model of the PMSM is always unstable around the trivial equilibrium point.

3. Global behavior of the PMSM

The fourth-order Runge–Kutta algorithm is employed in this part to construct the nonlinear analysis tools that are used to describe the overall behavior of the PMSM taken into consideration in this study. The variables and parameters of the motor are chosen in extended precision mode to ensure the accuracy of our computation. A fixed time step of 5×10^{-3} is employed for each iteration.

3.1. Two-dimensional dynamical maps

Using two-parameter Lyapunov diagrams, this section assesses the overall behavior of the PMSM under study. To generate the figure, two important dimensionless model parameters were concurrently changed, and the maximal Lyapunov exponent was noted after each iteration. These diagrams will be created in our example by modifying four important parameters of the investigated PMSM, namely b, ε, γ, and σ. When varying those parameters in the planes (σ, γ), (σ, ϵ), (σ, b), and (ϵ, b) Fig. 1 is obtained. These graphs are produced when both parameters are increased. It is evident from the diagrams in Fig. 2 that, depending on the sign of the highest Lyapunov exponent, the model

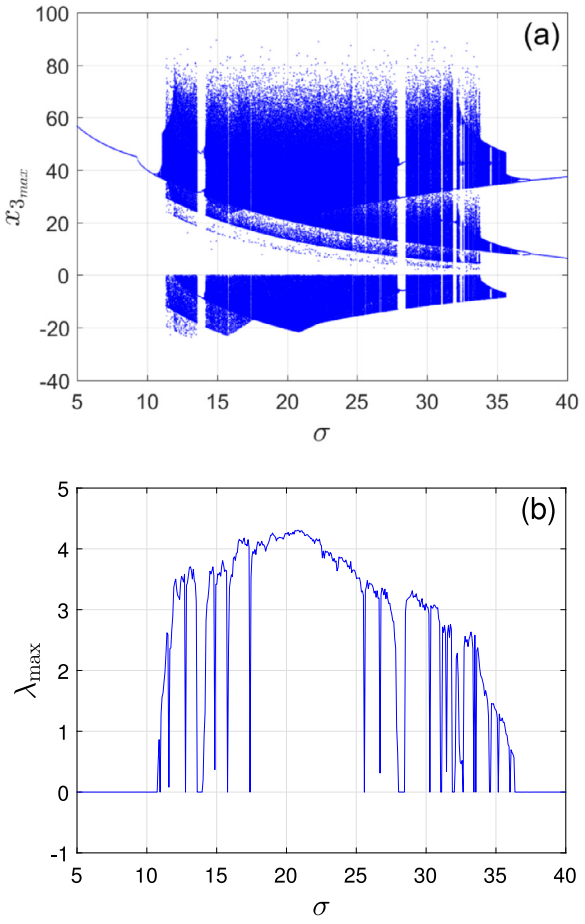

Fig. 2. (a) Bifurcation diagram showing the local maxima of the state variable $x_{3_{max}}$ when the control parameter σ is varied. (b) is the graph of the maximum Lyapunov exponent associated with (a). These diagrams are obtained for $b = 0.733, \epsilon = 0.0505$, and $\gamma = 350$.

under investigation is capable of exhibiting several types of dynamical behavior. For instance, Periodic behaviors are distinguished by $\lambda_{max} = 0$ whereas chaotic behaviors are distinguished by $\lambda_{max} > 0$. In addition, the absence of the negative Lyapunov exponent $\lambda_{max} < 0$ excludes the possibility of having resting behavior characterized by a stable state.

3.2. Coexistence of the bifurcations

The symmetric nature of the model is evident from the mathematical equation of the PMSM provided in Eq. (3). Consequently, (x_1, x_2, x_3) is also a solution for the identical set of parameters if $(-x_1, -x_2, -x_3)$ is a solution of system (3) for a given set of parameters. The bifurcation diagram of Fig. 2(a) shows how the considered model can move from periodic to periodic behavior through a wide range of chaotic behavior. Those transitions observed in the bifurcation diagram are well supported based on the graph of the maximum Lyapunov exponent in Fig. 2(b). Figs. 3(a) and (b) show enlargements of the bifurcation diagram of Fig. 2(a) on both sides. From those bifurcation diagrams, two sets of data are superimposed. Those superimposed data support the hysteretic dynamics of the considered PMSM. The graph of the Lyapunov exponent and the bifurcation diagrams in Fig. 4(a) and (b), respectively, have been calculated along the same lines. The figures in those diagrams have been computed by increasing or decreasing the control parameters. From those diagrams, the coexistence of periodic behavior and chaotic behavior for a large range of parameters has been observed. Those hysteretic dynamics are distinguished by the coexistence of several behaviors for the same set of parameters have been supported further by using the coexisting attractors of Fig. 5(a) and their basin of attraction of Fig. 5(b).

4. T-S fuzzy approach

Note that the arrangement alternates sporadically between negative and positive qualities. Despite the fact that the Lorenz conditions are completely predictable and the arrangement is entirely under the control of the underlying

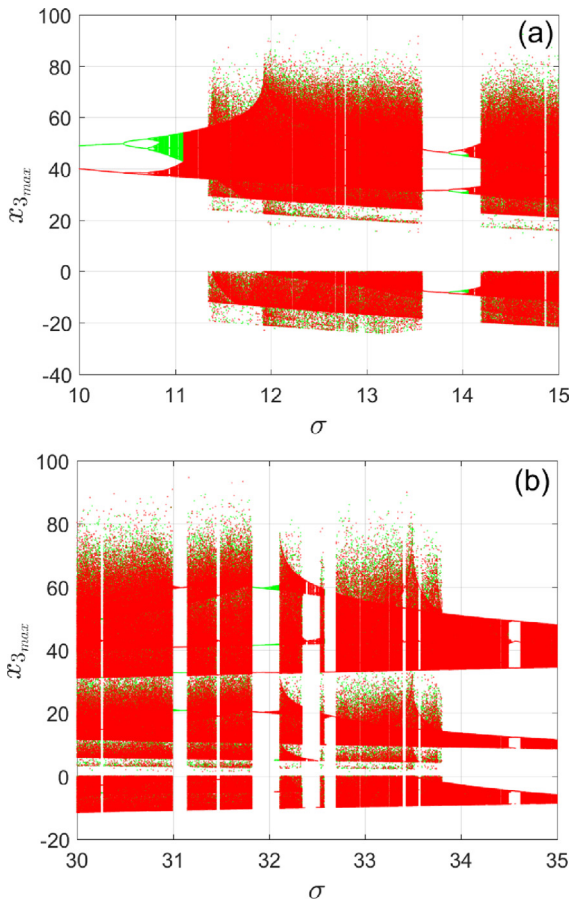

Fig. 3. Enlargement of the bifurcation diagram of Fig. 2. The red colors are obtained by decreasing the control parameters while the green color is obtained by increasing the control parameter.

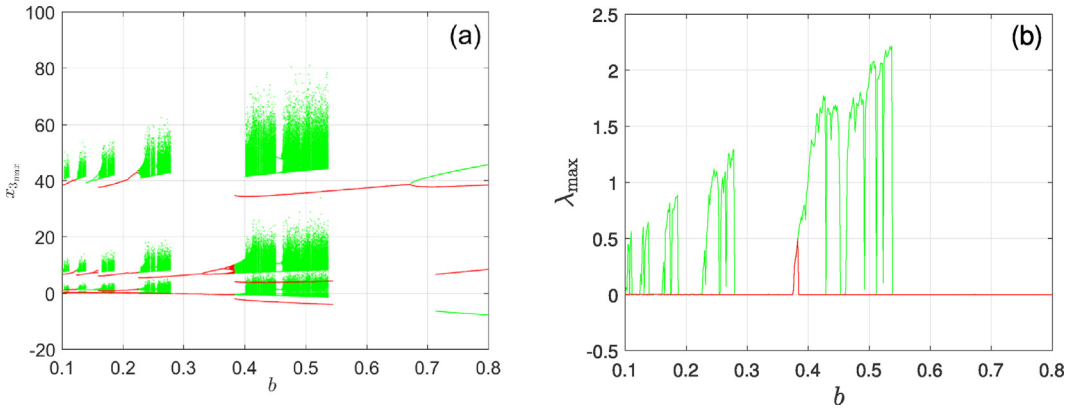

Fig. 4. (a) Bifurcation diagram showing the local maxima of the state variable $x_{3_{max}}$ when the control parameter b is varied. (b) is the graph of the maximum Lyapunov exponent associated with (a). These diagrams are obtained for $\sigma = 40$, $\epsilon = 0.1$, and $\gamma = 300$. These diagrams are obtained with the initial conditions $(0.1, 0, 4)$. The red colors are obtained by decreasing the control parameters while the blue color is obtained by increasing the control parameter.

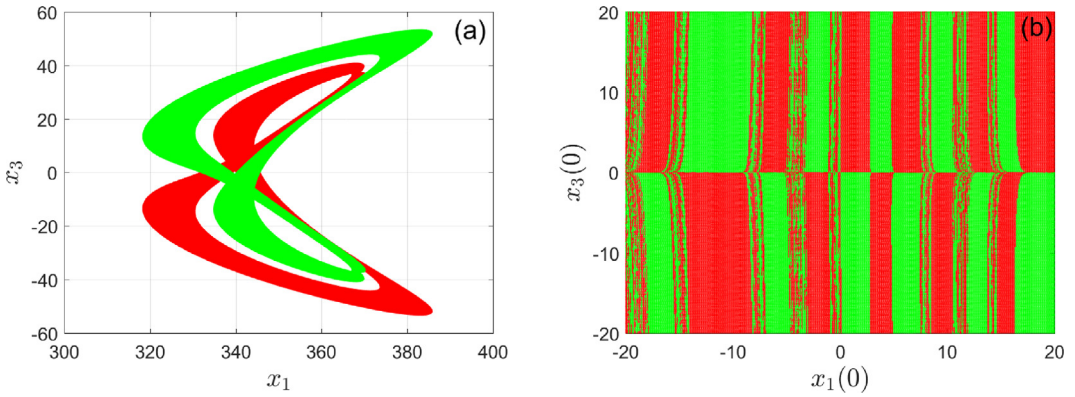

Fig. 5. (a) Phase trajectory showing the coexistence of the chaotic attractors. They are obtained with the parameter of Fig. 2. The attractor in red is obtained with the initials conditions $(0, 0, 4)$, while the one in green is obtained with the initial conditions $(0, 0, -4)$. (b) represents the cross-section of the basin of attraction of the coexisting trajectories in the plane $(x_1(0), x_3(0))$ for $x_2(0) = 0$.

circumstances, the chart of x vs t clearly resembles a random vibration. All things considered, the arrangement also exhibits particular normality in that the timing of the motion's recurrence and sufficiency is constant. The transformation $\hat{x} = [\hat{i}_d\ \hat{i}_q\ \bar{\omega}]^T$ is now applied to the entire matrix form of the examined model (1) for simulation purposes. The modified model is shown as

$$\begin{cases} \frac{di_d}{dt} = -i_d + \omega i_q + u_1, \\ \frac{di_q}{dt} = -i_q - \omega i_d + c\omega i_q + u_2, \\ \frac{d\omega}{dt} = a(i_q - \omega) + b i_d i_q - T_1 \end{cases} \tag{8}$$

with

$$a = \frac{L_q \beta \tilde{\theta}}{R_1 J},\ b = \frac{n_p \hat{b} \hat{k} \tilde{\theta}^2 (L_d - L_q)}{J},\ \hat{k} = \frac{\beta}{n_p \tilde{\theta} \psi_r},$$
$$\hat{b} = \frac{L_q}{L_d}, \tilde{\theta} = \frac{L_q}{R_1}, u_1 = \frac{1}{R_1 \hat{k}} u_d,\ T_1 = \frac{\tilde{\theta}^2}{J} T_L,\ c = -\frac{\psi_r}{\hat{k} L_q},$$
$$\hat{x} = [\hat{i}_d,\ \hat{i}_q\ \hat{\omega}]^T, u_2 = \frac{1}{R_1 \hat{k}} u_q.$$

For convenience, we denote $i_d = \hat{i}_d\ i_q = \hat{i}_q\ \omega = \bar{\omega}$, and $x = \hat{x}$. The approximate linear subsystems of the studied nonlinear system might be depicted by a T-S fuzzy model defined by the following **IF** $-$ **THEN** rules: *Plant Rule* i : **IF** $z_1(t)$ is F_{i1}, $z_2(t)$ is F_{i2}, and ... and $z_p(t)$ is F_{ip}, **THEN**

$$\dot{x}(t) = A_i x(t) + B_i u(t) + E_i w(t). \tag{9}$$

In this case, the fuzzy sets are $F_{ij} (i = 1, 2, \ldots, r, j = 1, 2, \ldots, p)$, the premise variables are $z_1(t), z_2(t), \ldots, z_j(t) (j = 1, 2, \ldots, p)$, and the number of IF-THEN rules is r. The state, control input, and bounded peak disturbance are denoted by $x(t) \in \mathbb{R}^n$, $u(t) \in \mathbb{R}^m$, and $w(t) \in \mathbb{R}^l$, respectively. Real constant matrices with compatible dimensions are A_i, B_i, and E_i. Additionally, the disturbance $w(t)$ meets the condition

$$w^T(t) w(t) \leq \hat{w}^2. \tag{10}$$

The following is a description of (9) with center-average defuzzier, product inference, and singleton fuzzifier:

$$\dot{x}(t) = \sum_{i=1}^{4} h_i(z(t)) \Big\{ A_i x(t) + B_i u(t) + E_i w(t) \Big\}. \tag{11}$$

with

$$A_1 = \begin{bmatrix} -a & 0 & a + bW_1 \\ 0 & -\frac{L_q}{L_d} & W_2 \\ c & -W_2 & -1 \end{bmatrix},$$

$$A_2 = \begin{bmatrix} -a & 0 & a - bW_1 \\ 0 & -\frac{L_q}{L_d} & -W_2 \\ c & W_2 & -1 \end{bmatrix},$$

$$A_3 = \begin{bmatrix} -a & 0 & a + bW_1 \\ 0 & -\frac{L_q}{L_d} & -W_2 \\ c & W_2 & -1 \end{bmatrix},$$

$$A_4 = \begin{bmatrix} -a & 0 & a - bW_1 \\ 0 & -\frac{L_q}{L_d} & W_2 \\ c & -W_2 & -1 \end{bmatrix},$$

$$B_i = [1\ 1\ 0]^T,\ E_i = [0\ 0\ T_1]^T.$$

The membership functions are

$$h_1(z(t)) = H_{11}(i_d(t)).H_{21}(\omega(t)),$$
$$h_2(z(t)) = H_{12}(i_d(t)).H_{22}(\omega(t)),$$
$$h_3(z(t)) = H_{11}(i_d(t)).H_{22}(\omega(t)),$$
$$h_4(z(t)) = H_{12}(i_d(t)).H_{21}(\omega(t)).$$

Here

$$H_{11}(i_d(t)) = 0.5\left(1 + \frac{i_d(t)}{W_1}\right), H_{21}(\omega(t)) = 0.5\left(1 + \frac{\omega(t)}{W_2}\right),$$
$$H_{12}(i_d(t)) = 0.5\left(1 - \frac{i_d(t)}{W_1}\right), H_{22}(\omega(t)) = 0.5\left(1 - \frac{\omega(t)}{W_2}\right).$$

Denote $z(t) = [z_1(t)\ z_2(t)\ \cdots\ z_p(t)]^T$ and

$$h_i(z(t)) = \frac{\mu_i(z(t))}{\sum_{i=1}^{r} \mu_i(z(t))},\ \mu_i(z(t)) = \prod_{j=1}^{p} F_{ij}(z_j(t)),$$

where the grade memberships of $z_j(t)$ in F_{ij} are represented by $F_{ij}(z_j(t))$. It is clear that for every t, $\mu_i(z(t)) \geq 0$. As a result, it can be proven that for every $t > 0$, $\sum_{i=1}^{r} h_i(z(t)) = 1$ and $h_i(z(t)) \geq 0$. Additionally, 1 and 12 are selected as the values of W_1 and W_2, respectively.

5. Sampled-data controller

The measurement $x(t_k)$, which is a discrete-time control of $x(t)$ at the sampling instant t_k, is presumed to be the only one that can be obtained for control purposes. A zero-order holder (ZOH) with a sequence of hold times provides the control signal.

$$0 = t_0 < t_1 < \cdots < t_k \cdots < \lim_{k \to +\infty} t_k = +\infty.$$

Based on parallel distributed compensation (PDC), we use the fuzzy SDC for (9). Its fuzzy sets match the fuzzy model's premise components. The schematic of fuzzy NFSDC is shown in Fig. 6.

Controller Rule j:
IF $z_1(t)$ is F_{j1}, $z_2(t)$ is F_{j2}, and ... and $z_p(t)$ is F_{jp},
THEN

$$u(t) = (\mathcal{K}_j + \triangle\mathcal{K}_j(t))x(t_k),\ t \in [t_k, t_{k+1}) \tag{12}$$

where $\mathcal{K}_j \in R^{m \times n} (j = 1, 2, \ldots, 4)$ is the gain matrix of the controller, and $\triangle\mathcal{K}_j(t)$ is the unknown matrix representing gain disturbances and satisfies

$$\triangle\mathcal{K}_j(t) = \mathcal{H}_{1j}\mathcal{G}_{1j}(t)\mathcal{M}_{1j},$$

where $\mathcal{H}_{1j}$ and $\mathcal{M}_{1j}$ denote known matrices, and $\mathcal{G}_{1j}(t)$ denotes the unknown matrix function and fulfills $\mathcal{G}_{1j}^{\top}(t)\mathcal{G}_{1j}(t) \leq I$. Consequently, fuzzy SDC is defined by

$$u(t) = \sum_{j=1}^{4} h_j(z(t_k))(\mathcal{K}_j + \triangle\mathcal{K}_j(t))x(t_k). \tag{13}$$

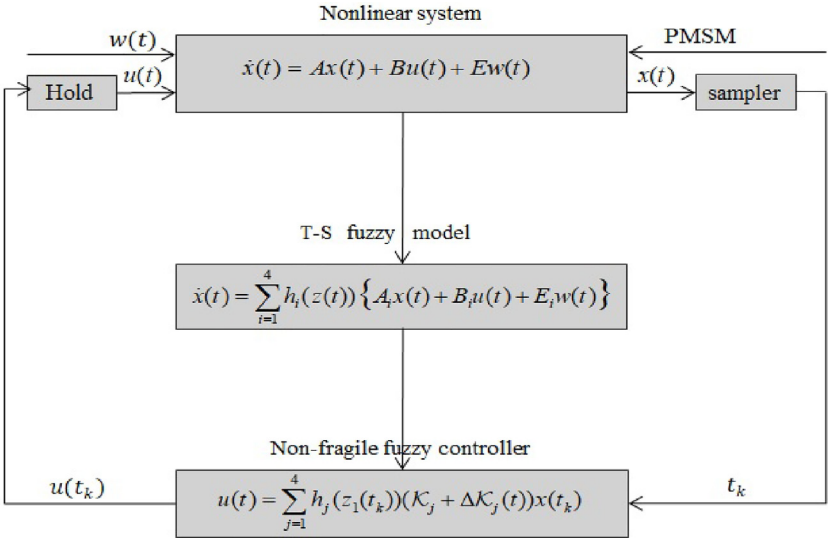

Fig. 6. Block diagram for fuzzy NFSDC (14).

Given that $t_k \leq t < t_{k+1}$ and $h_k = t_{k+1} - t_k$, indicate the sampling interval as $\eta(t) = t - t_k$. It is obvious that $0 \leq \eta(t) < h_k \leq \bar{h}$, where $\bar{h} > 0$ is a given scalar and denotes the maximum upper bound of sampling instant. Additionally, the derivative of $\eta(t)$ is piecewise linear and has the value $\dot{\eta}(t) = 1, t \neq t_k$. Substituting (13) into (11), the closed-loop uncertain T-S fuzzy system is obtained as follows

$$\dot{x}(t) = \sum_{i=1}^{4}\sum_{j=1}^{4} h_i(z(t))h_j(z(t_k))\Big[A_i x(t) + B_i(\mathcal{K}_j + \triangle\mathcal{K}_j(t))x(t_k) + E_i w(t)\Big]. \tag{14}$$

The following definition and lemmas, which are required in the derivations of our key conclusions, are introduced before this section is concluded.

Definition 5.1 ([34]). The reachable set of system (14) is shown as follows for $\forall t \geq 0$,

$$\mathcal{R}_x = \{x(t) \mid x(t) \text{ and } w(t) \text{ satisfy (14) with (10)}\}, \tag{15}$$

and an ellipsoid used to bound the reachable set system (14) and describing $\epsilon(\mathcal{P}) = \{x(t) \in \mathbb{R}^n \mid x(t)^T \mathcal{P} x(t) \leq 1, \mathcal{P} > 0\}$.

Lemma 5.2 ([34]). *Let $V(x(t))$ be a differentiable Lyapunov function with $V(x(0)) = 0$ and $w(t)$ satisfying (10). If there exists a scalar $\alpha > 0$ such that $\dot{V}(x(t)) + 2\alpha V(t) - \frac{\alpha}{\hat{w}^2} w^T(t)w(t) \leq 0$, then $V(x(t)) \leq 1$.*

Lemma 5.3 ([36]). *For every matrix $R > 0$, any vector ξ, and any continuously differentiable function $x : [-\tau, 0] \to R^n$, and slack matrices $\mathcal{M}, \mathcal{N}$, it holds*

$$\begin{aligned}
&-\tau \int_{t-\tau}^{t} \dot{x}^\top(s) R \dot{x}(s) ds \\
&\leq \xi^\top(t)[\tau(t) M^\top \hat{R}^{-1} M + h_\tau N^\top \hat{R}^{-1} N] \\
&+ \Big(\frac{h_\tau}{\tau} + \frac{\tau(t)^2}{\tau^2}\Big) Sym[\nu^\top(t - \tau(t), t)\Gamma_a^\top M \\
&+ \nu^\top(t - \tau, t - \tau(t))\Gamma_a^\top N]\xi(t) \\
&- \Big\{\frac{h_\tau}{\tau}\nu^\top(t - \tau(t), t)\Gamma_a^\top M \hat{R} \Gamma_a \nu(t - \tau(t), t) \\
&+ \frac{\tau(t)^2}{\tau^2}\nu^\top(t - \tau, t - \tau(t))\Gamma_a^\top M \hat{R} \Gamma_a (t - \tau, t - \tau(t))\Big\}.
\end{aligned}$$

where

$$\hat{R} = diag\{R, 3R, \ldots, (2S+1)R\},$$
$$\Gamma_a = col[\pi_s(0), \pi_s(1), \ldots, \pi_s(S)],$$
$$\xi(t) = col[x(t), x(t-\tau(t)), x(t-\tau), \dot{x}(t-\tau(t)), \dot{x}(t-\tau),$$
$$\omega_1(t-\tau(t), t), \omega_1(t-\tau, t-\tau(t)), \omega_2(t-\tau(t), t),$$
$$\omega_2(t-\tau, t-\tau(t))], \omega_1(a,b) = \frac{1}{(b-a)}\int_a^b x(s)ds,$$
$$\omega_1(a,b) = \frac{1}{(b-a)^2}\int_a^b\int_u^b x(s)dsdu.$$

Lemma 5.4 (*[37]*). *For any semi-positive definite matrices* $U = \begin{bmatrix} \mathcal{U}_{11} & \mathcal{U}_{12} & \mathcal{U}_{13} \\ \mathcal{U}_{12}^\top & \mathcal{U}_{22} & \mathcal{U}_{23} \\ \mathcal{U}_{13}^\top & \mathcal{U}_{23}^\top & \mathcal{U}_{33} \end{bmatrix} \geq 0$ *the subsequent integral inequality satisfies:*

$$-\int_{t-d(t)}^{t} \dot{\xi}^T(s)U_{33}\dot{\xi}(s)ds \leq \int_{t-d(t)}^{t} [\xi^T(t)\ \xi^T(t-d(t))\ \dot{\xi}^\top(s)]$$
$$\begin{bmatrix} \mathcal{U}_{11} & \mathcal{U}_{12} & \mathcal{U}_{13} \\ \mathcal{U}_{12}^\top & \mathcal{U}_{22} & \mathcal{U}_{23} \\ \mathcal{U}_{13}^\top & \mathcal{U}_{23}^\top & 0 \end{bmatrix} \begin{bmatrix} \xi(t) \\ \xi(t-d(t)) \\ \dot{\xi}(s) \end{bmatrix} ds.$$

Lemma 5.5. *Let* $J(t)$ *meet the condition that* $J^T(t)J(t) \leq I$, *and let* Y, ξ, *and* $J(t)$ *be real matrices of the proper dimensions. Then, for every constant* $\epsilon > 0$, *the following inequality is true:*

$$YJ(t)\xi + \xi^T J^T(t)Y^T \leq \epsilon YY^T + \epsilon^{-1}\xi^T\xi.$$

6. Main results

The RSE and synthesis for the T-S fuzzy system (14) with a non-fragile sampled-data control (NFSDC) design and bounded peak disturbance fulfilling $w^T(t)w(t) \leq \hat{w}^2$ will be shown in this part. First off, using the given $\mathcal{K}_j$, the RSE problem may be resolved in terms of LMIs. We denote matrices for simplicity,

$$e_l = [0_{n\times(l-1)n}\ I_n\ 0_{n\times(10-1)n}]^\top, l = 1, 2, \ldots, 10,\ \boldsymbol{h} = e^{-2\alpha\bar{h}}$$
$$\mathcal{S} = \begin{bmatrix} \mathcal{S}_1 & \mathcal{S}_2 \\ * & \mathcal{S}_3 \end{bmatrix}, \mathcal{F} = \begin{bmatrix} \dot{x}(s) \\ x(t_k) \end{bmatrix}, \eta(t) = \bar{d}, \bar{h}_d = \bar{h} - \bar{d}.$$

Theorem 6.1. *Given the positive scalar* $\alpha, \bar{h}, \emptyset_i > 0$, *and gain matrices* $\mathcal{K}_j$, *such that the considered reachable set of the closed-loop system (14) is bounded by condition (15), if there exist positive definite matrices* $\mathcal{P} > 0, \mathcal{S}_1 > 0, \mathcal{S}_2 > 0, \mathcal{S}_3 > 0, \mathcal{T} > 0$, *matrices* $\mathcal{Y}_1$ *and* $\mathcal{Y}_2$, *semi-positive definite matrices* $\mathcal{U} = [\mathcal{U}_{mn}]_{3\times3} \geq 0$, *matrices* $\mathcal{W}_l (l = 1, 2, 3)$, *such that the following LMIs hold with* $\eta(t) = \{0, \bar{h}\}$:

$$\begin{bmatrix} \hat{\Xi}_{ij}(0) & \sqrt{\bar{h}}\mathcal{Y}_2^\top & \mathcal{O}_{1ij}^\top & \emptyset_i\mathcal{O}_{2ij}^\top \\ * & -\mathcal{S}_1 & 0 & 0 \\ * & * & -\emptyset_i I & 0 \\ * & * & * & -\emptyset_i I \end{bmatrix} < 0, \tag{16}$$

$$\begin{bmatrix} \hat{\Xi}_{ij}(\bar{h}) & \sqrt{\bar{h}}\mathcal{Y}_1^\top & \mathcal{O}_{1ij}^\top & \emptyset_i\mathcal{O}_{2ij}^\top \\ * & -\mathcal{S}_1 & 0 & 0 \\ * & * & -\emptyset_i I & 0 \\ * & * & * & -\emptyset_i I \end{bmatrix} < 0, \tag{17}$$

$$\begin{bmatrix} -\bar{h}^2\tilde{\phi} + \hat{\Xi}_{ij}(0) & \sqrt{\bar{h}}\mathcal{Y}_2^\top & \mathcal{O}_{1ij}^\top & \emptyset_i\mathcal{O}_{2ij}^\top \\ * & -\mathcal{S}_1 & 0 & 0 \\ * & * & -\emptyset_i I & 0 \\ * & * & * & -\emptyset_i I \end{bmatrix} < 0, \tag{18}$$

where

$$\begin{aligned}
\hat{\Xi}_{ij}(\bar{d}) &= \hat{\Xi}_{01}(\bar{d}) + \hat{\Xi}_{02}(\bar{d}),\\
\hat{\Xi}_{01}(\bar{d}) &= \chi_1 + \chi_2 + \chi_3 + \chi_4 + \bar{\Omega}_{3ij} + e_{10}^T \frac{-\alpha}{\hat{w}^2} e_{10},\\
\hat{\Xi}_{02}(\bar{d}) &= (\frac{\bar{h}_d}{\bar{h}} + \frac{\bar{d}^2}{\bar{h}^2}) Sym[\mathcal{Y}_1\mathcal{X}_1 + \mathcal{Y}_2\mathcal{X}_2]\\
&\quad - (\frac{\bar{h}_d}{\bar{h}^2}\mathcal{X}_1^\top S_1 \mathcal{X}_1 + \frac{\bar{d}}{\bar{h}^2}[\mathcal{X}_2^\top S_1 \mathcal{X}_2)],\\
\mathcal{X}_1 &= col[e_1 - e_2, e_1 + 2_2 - 2e_6, e_1 - e_2 + 6e_6 - 12e_8],\\
\mathcal{X}_2 &= col[e_2 - e_3, e_2 + e_3 - 2e_7, e_2 - e_3 = 6e_7 - 12e_9],\\
\tilde{\phi} &= \frac{1}{\bar{h}^2} Sym[\mathcal{Y}_1\mathcal{X}_1 + \mathcal{Y}_2\mathcal{X}_2], \mathcal{S}_1 = diag\{\mathcal{S}_1, 3\mathcal{S}_1, 5\mathcal{S}_1\},\\
\chi_1 &= Sym\{\alpha e_1 \mathcal{P} e_1^\top + e_1 \mathcal{P} e_5^\top\},\\
\chi_2 &= -\mathbf{h}(2(e_2 - e_4)^\top \mathcal{S}_2 e_4 + \bar{h} e_4^\top \mathcal{S}_3 e_4) + \bar{h}\mathcal{F}^\top \mathcal{S}\mathcal{F} + \hat{\Xi}_{02}(\bar{d}),\\
\chi_3 &= e_1^\top[\bar{h}\mathcal{U}_{11} + 2\mathcal{U}_{13}]e_1 + 2e_1^\top[\bar{h}\mathcal{U}_{12} - \mathcal{U}_{13} + \mathcal{U}_{13}^\top]e_3\\
&\quad + e_3^\top[\bar{h}\mathcal{U}_{22} - \mathcal{U}_{23} + \mathcal{U}_{23}^\top]e_3,\\
\chi_4 &= \bar{h} e_5^\top \mathcal{T} e_5 + \mathbf{h}\chi_3,\\
\bar{\Omega}_{3ij} &= -e_1^\top \mathcal{W}_1 e_5 + 2e_1^\top \mathcal{W}_1^\top A_i e_1 + e_1^\top \mathcal{W}_1^\top B_i \mathcal{K}_j e_4\\
&\quad - 2e_5^\top \mathcal{W}_2^\top e_5 + e_1^\top A_i^\top \mathcal{W}_2 e_5 + e_4^\top \mathcal{K}_j^\top B_i^\top \mathcal{W}_2 e_5\\
&\quad - e_4^\top \mathcal{W}_3^\top e_5 + e_1^\top A_i^\top \mathcal{W}_3 e_4 + 2e_4^\top \mathcal{W}_3^\top B_i \mathcal{K}_j e_4\\
&\quad - e_1^T \mathcal{W}_1 E_i e_{10} + e_5^T \mathcal{W}_2 E_i e_{10} + e_4^T \mathcal{W}_3 E_i e_{10},\\
\eth_{1ij} &= [\mathcal{H}_{1j}\mathcal{W}_1\ 0\ 0\ \mathcal{H}_{1j}\mathcal{W}_3\ \mathcal{H}_{1j}\mathcal{W}_2\ 0_{1\times 5}],\\
\eth_{2ij} &= [0\ 0\ 0\ \mathcal{M}_{1j}\mathcal{K}_j\ 0_{1\times 6}].
\end{aligned}$$

Then the reachable set of system (14) are bounded $\epsilon(\mathcal{P})$ *such that* $\{x(t) \in \mathbb{R}^n \mid \|x(t)\| \le \hat{r}\}$ *with* $\hat{r} = \frac{1}{\sqrt{\lambda_{min}(\mathcal{P})}}$.

Proof. Take into consideration the LKF for the system (14) shown below:

$$V(t) = \sum_{l=1}^{3} V_l(t), t \in [t_k, t_{k+1}) \tag{19}$$

where

$$\begin{aligned}
V_1(t) &= x^\top(t)\mathcal{P}x(t),\\
V_2(t) &= (t_{k+1} - t)\int_{t-\bar{h}}^{t} e^{2\alpha(s-t)}\mathcal{F}^\top \mathcal{S}\mathcal{F} ds,\\
V_3(t) &= (t_{k+1} - t)\int_{t-\bar{h}}^{t} e^{2\alpha(s-t)}\dot{x}^\top(s)\mathcal{T}\dot{x}(s) ds,
\end{aligned} \tag{20}$$

By combining the system (14) state trajectories with the time derivative of $V(t)$, we obtain

$$\begin{aligned}
\dot{V}_1(t) + 2\alpha V_1(t) &= 2x^\top(t)\mathcal{P}\dot{x}(t) + 2\alpha x^\top(t)\mathcal{P}x(t),\\
&= \xi^\top(t)\chi_1\xi(t),
\end{aligned} \tag{21}$$

$$\begin{aligned}
\dot{V}_2(t) + 2\alpha V_2(t) &= (t_{k+1} - t)\mathcal{F}^\top \mathcal{S}\mathcal{F} - \int_{t-\bar{h}}^{t} e^{-2\alpha\bar{h}}\mathcal{F}^\top \mathcal{S}\mathcal{F} ds\\
&\le (t_{k+1} - t)\mathcal{F}^\top \mathcal{S}\mathcal{F} - e^{-2\alpha\bar{h}}\Big\{\int_{t-\bar{h}}^{t} \dot{x}^\top(s)\mathcal{S}_1\dot{x}(s) ds\\
&\quad - (t - t_k)x^T(t_k)\mathcal{S}_3 x(t_k) - 2(x(t) - x(t_k))^T \mathcal{S}_2 x(t_k)\Big\}.
\end{aligned} \tag{22}$$

By using the inequality in Lemma 5.3, we have

$$
\begin{aligned}
&-\int_{t-\bar{h}}^{t}\dot{x}^{\top}(s)\mathbb{S}_1\dot{x}(s)ds \le \xi^{\top}(t)[\bar{d}\mathcal{Y}_1^{\top}\mathbb{S}_1^{-1}\mathcal{Y}_1\\
&+\bar{h}_d\mathcal{Y}_2^{\top}\mathbb{S}_1^{-1}\mathcal{Y}_2+(\frac{\bar{h}_d}{\bar{h}}+\frac{\bar{d}^2}{\bar{h}^2})Sym[\mathcal{Y}_1\mathcal{X}_1+\mathcal{Y}_2\mathcal{X}_2]\\
&-(\frac{\bar{h}_d}{\bar{h}^2}\mathcal{X}_1^{\top}\mathbb{S}_1\mathcal{X}_1+\frac{\bar{d}}{\bar{h}^2}\mathcal{X}_2^{\top}\mathbb{S}_1\mathcal{X}_2)]\xi^{\top}(t),\\
&\le \xi^{\top}(t)[\Xi_{11}(\bar{d})+\Xi_{12}(\bar{d})]\xi(t),
\end{aligned}
\tag{23}
$$

$$
\begin{aligned}
\dot{V}_2(t)+2\alpha V_2(t) &\le e^{-2\alpha\bar{h}}(-(t-t_k)x^T(t_k)\mathbb{S}_3x(t_k)\\
&-2(x(t)-x(t_k))^T\mathbb{S}_2x(t_k)-\xi^{\top}(t)[\Xi_{11}(\bar{d})+\Xi_{12}(\bar{d})]\xi(t))\\
&+(t_{k+1}-t)F^{\top}\mathbb{S}F,\\
&\le \xi^{\top}(t)\chi_2\xi(t),
\end{aligned}
\tag{24}
$$

$$
\begin{aligned}
\dot{V}_3(t)+2\alpha V_3(t) &\le (t_{k+1}-t)\dot{x}^{\top}(t)\mathcal{T}\dot{x}(t)\\
&-\int_{t-\bar{h}}^{t}e^{2\alpha(s-t)}\dot{x}^{\top}(s)\mathcal{T}\dot{x}(s)ds,\\
&\le (t_{k+1}-t)\dot{x}^{\top}(t)\mathcal{T}\dot{x}(t)-\int_{t-\bar{h}}^{t}e^{2\alpha\bar{h}}\dot{x}^{\top}(s)\mathcal{T}\dot{x}(s)ds.
\end{aligned}
\tag{25}
$$

From $\dot{V}_3(t)$, the following equations hold

$$
\begin{aligned}
&-\int_{t-\bar{h}}^{t}\dot{x}^{\top}(s)\mathcal{T}\dot{x}(s)ds=-\int_{t-\bar{h}}^{t}\dot{x}^{\top}(s)\mathcal{U}_{33}\dot{x}(s)ds\\
&-\int_{t-\bar{h}}^{t}\dot{x}^{\top}(s)[\mathcal{T}-\mathcal{U}_{33}]\dot{x}(s)ds.
\end{aligned}
\tag{26}
$$

Applying Lemma 5.4 and the LeibnizNewton formula for the integral term in (26) such as $-\int_{t-\bar{h}}^{t}\dot{x}^{\top}(s)\mathcal{U}_{33}\dot{x}(s)ds$; the following equations hold for any matrix $\mathcal{U}$ with appropriate dimensions, respectively. Thus, we obtain the following.

$$
\begin{aligned}
&-\int_{t-\bar{h}}^{t}\dot{x}^{\top}(s)\mathcal{U}_{33}\dot{x}(s)ds\le\int_{t-\bar{h}}^{t}\mathcal{I}_{11}^{\top}\mathcal{I}_{12}\mathcal{I}_{11}ds\\
&\le x^{\top}(t)[\bar{h}\mathcal{U}_{11}+2\mathcal{U}_{13}]x(t)+2x^{\top}(t)[\bar{h}\mathcal{U}_{12}-\mathcal{U}_{23}+\mathcal{U}_{13}^{\top}]\\
&\times x(t-\bar{h})+x^{\top}(t-\bar{h})[\bar{h}\mathcal{U}_{22}-\mathcal{U}_{23}+\mathcal{U}_{23}^{\top}]x(t-\bar{h}),\\
&\le \xi^{\top}(t)\chi_3\xi(t).
\end{aligned}
\tag{27}
$$

where

$$
\mathcal{I}_{11}^{\top}=[x^T(t)\;x^T(t-\bar{h})\;\dot{x}^{\top}(s)]
$$

$$
\mathcal{I}_{12}=\begin{bmatrix}\mathcal{U}_{11}&\mathcal{U}_{12}&\mathcal{U}_{13}\\ \mathcal{U}_{12}^{\top}&\mathcal{U}_{22}&\mathcal{U}_{23}\\ \mathcal{U}_{13}^{\top}&\mathcal{U}_{23}^{\top}&0\end{bmatrix}.
$$

Therefore, we get the following.

$$
\begin{aligned}
\dot{V}_3(t)+2\alpha V_3(t) &\le (t_{k+1}-t)\dot{x}^{\top}(t)\mathcal{T}\dot{x}(t)+\xi^{\top}(t)\chi_3\xi(t)\\
&-\int_{t-\bar{h}}^{t}\dot{x}^{\top}(s)[\mathcal{T}-\mathcal{U}_{33}]\dot{x}(s)ds,\\
&\le \xi^{\top}(t)\chi_4\xi(t),
\end{aligned}
\tag{28}
$$

For any real matrix $\mathcal{W}_l(l=1,2,3)$, we have the following inequalities:

$$
\begin{aligned}
0=Sym\Big[x^{\top}(t)\mathcal{W}_1+\dot{x}^{\top}(t)\mathcal{W}_2+x^{\top}(t_k)\mathcal{W}_3\Big]\Big[-\dot{x}(t)\\
+\sum_{i=1}^{r}\sum_{j=1}^{r}h_i(z(t))h_j(z(t_k))[A_ix(t)+B_i\mathcal{K}_jx(t_k)+E_iw(t)]\Big],
\end{aligned}
$$

$$
\begin{aligned}
&= \sum_{i=1}^{r}\sum_{j=1}^{r} h_i(z(t))h_j(z(t_k))Sym\Big[x^\top(t)\mathcal{W}_1 + \dot{x}^\top(t)\mathcal{W}_2 \\
&\quad + x^\top(t_k)\mathcal{W}_3\Big]\Big[-\dot{x}(t) + A_i x(t) + B_i\mathcal{K}_j x(t_k) + E_i w(t)\Big], \\
&= \{\bar{\Omega}_{3ij} + Sym\{\eth_{1ij}^\top \mathcal{G}_{1j}\eth_{2ij}\}\}. \qquad (29)
\end{aligned}
$$

From Lemma 5.5, it can be verified that

$$
sym\{\eth_{1ij}^\top \mathcal{G}_{1j}\eth_{2ij}\} \le \frac{1}{\emptyset}\eth_{1ij}^\top\eth_{1ij} + \emptyset\eth_{2ij}^\top\eth_{2ij}. \qquad (30)
$$

Combining (20)–(30), we get

$$
\begin{aligned}
&\dot{V}(t) + 2\alpha V(t) - \frac{\alpha}{\tilde{w}^2} w^T(t)w(t) < \xi^\top(t)[\hat{\Xi}_{*ij} \\
&\quad + \bar{d}\mathcal{Y}_1^\top S_1^{-1}\mathcal{Y}_1 + \bar{h}_d\mathcal{Y}_2^\top S_1^{-1}\mathcal{Y}_2]\xi(t) < 0. \qquad (31)
\end{aligned}
$$

where, $\xi^\top(t) = [x^\top(t), x^\top(t-\bar{d}), x^\top(t-\bar{h}), x^\top(t_k),\ \dot{x}^\top(t),\ \frac{1}{\eta(t)}\int_{t-\eta(t)}^{t} x^\top(s)ds,\ \frac{1}{\bar{h}-\eta(t)}\int_{t-\bar{h}}^{t-\eta(t)} x^\top(s)ds,\ \frac{1}{\eta(t)^2}\int_{t-\eta(t)}^{t}\times\int_{u}^{t} x^\top(s)dsdu$, $\frac{1}{(\bar{h}-\eta(t))^2}\int_{t-\bar{h}}^{t-\eta(t)}\int_{u}^{t-\eta(t)} x^\top(s)dsdu,\ w^\top(t)]$ and $\hat{\Xi}_{*ij} = \hat{\Xi}_{01}(\bar{d}) + \frac{1}{\emptyset_i}\eth_{1ij}^\top\eth_{1ij} + \emptyset_i\eth_{2ij}^\top\eth_{2ij}$. where $\hat{\Xi}_{01}(\bar{d})$ is defined in Theorem 6.1. Since $\mathcal{T} - \mathcal{U}_{33} \ge 0$ then the last terms in (26) is less than or equal to 0. Furthermore, using the Schur complement, it is guaranteed to see Eqs. (16)(18). Thus according to Lemma 5.2, one has $V(t) \le 1$. It is easy to see

$$
x^\top(t)\mathcal{P}x(t) = V_1(t) \le V_1(t) + V_2(t) + V_3(t) = V(t).
$$

Moreover, by using the spectral property for symmetric positive definite matrix $\mathcal{P}$, we get

$$
\lambda_{min}(\mathcal{P})\|x(t)\|^2 \le V(t). \qquad (32)
$$

Therefore, $\|x(t)\| \le \hat{r} = \frac{1}{\sqrt{\lambda_{min}(\mathcal{P})}}$ due to (32). This means that the reachable set of the system (14) is bounded by $\epsilon(P) = \{x(t) \in \mathcal{R}^n \mid x^T(t)\mathcal{P}x(t) \le 1\}$ based on Definition 5.1. The proof is completed. □

Remark 6.2. It should be worth mentioning that the design of the LKF $V_2(t) = (t_{k+1} - t)\int_{t-\bar{h}}^{t} e^{2\alpha(s-t)}F^\top\mathcal{S}Fds$, $V_3(t) = (t_{k+1} - t)\int_{t-\bar{h}}^{t} e^{2\alpha(s-t)}\dot{x}^\top(s)\mathcal{T}\dot{x}(s)ds$ based on the NFSDC information $t_k \le t < t_{k+1}$ and $h_k = t_{k+1} - t_k$, indicate the sampling interval as $\eta(t) = t - t_k$. It is obvious that $0 \le \eta(t) < h_k \le \bar{h}$ and utilize these sampling intervals the $V_2(t)$ and $V_3(t)$ is similar to $(t_{k+1} - t)\int_{t_k}^{t} e^{2\alpha(s-t)}F^\top\mathcal{S}Fds$ and $(t_{k+1} - t)\int_{t_k}^{t} e^{2\alpha(s-t)}\dot{x}^\top(s)\mathcal{T}\dot{x}(s)ds$ with $\lim_{t\to t_k} V_2(t) = V_2(t_k) = 0$ and $\lim_{t\to t_k} V_3(t) = V_3(t_k) = 0$ which has been also used to prove the reachable set synthesis of the proposed LKF in Theorem 6.1.

Theorem 6.3. *Given the positive scalar $\alpha, \bar{h}, \emptyset_i > 0, k_l(l = 1, 2, 3)$, such that the considered reachable set of the closed-loop system (14) is bounded by condition (15), if there exist positive definite matrices $\tilde{\mathcal{P}} > 0, \tilde{\mathcal{S}}_1 > 0, \tilde{\mathcal{S}}_2 > 0, \tilde{\mathcal{S}}_3 > 0, \tilde{\mathcal{T}} > 0$, matrices $\tilde{\mathcal{Y}}_1, \tilde{\mathcal{Y}}_2$, semipositive definite matrices $\tilde{\mathcal{U}} = [\tilde{\mathcal{U}}_{mn}]_{3\times3} \ge 0$, matrices $\mathbb{Y}_j$ and $\mathbb{W}$, such that the following conditions are satisfied for any $\eta(t) = \{0, \bar{h}\}$*

$$
\begin{bmatrix}
\widehat{\Xi}_{ij}(0) & \sqrt{\bar{h}}\tilde{\mathcal{Y}}_2^\top & \tilde{\eth}_{1ij}^\top & \emptyset_i\tilde{\eth}_{2ij}^\top \\
* & -\tilde{\mathcal{S}}_1 & 0 & 0 \\
* & * & -\emptyset_i I & 0 \\
* & * & * & -\emptyset_i I
\end{bmatrix} < 0, \qquad (33)
$$

$$
\begin{bmatrix}
\widehat{\Xi}_{ij}(\bar{h}) & \sqrt{\bar{h}}\tilde{\mathcal{Y}}_1^\top & \tilde{\eth}_{1ij}^\top & \emptyset_i\tilde{\eth}_{2ij}^\top \\
* & -\tilde{\mathcal{S}}_1 & 0 & 0 \\
* & * & -\emptyset_i I & 0 \\
* & * & * & -\emptyset_i I
\end{bmatrix} < 0, \qquad (34)
$$

$$
\begin{bmatrix}
-\bar{h}^2\tilde{\phi} + \widehat{\Xi}_{ij}(0) & \sqrt{\bar{h}}\tilde{\mathcal{Y}}_2^\top & \tilde{\eth}_{1ij}^\top & \emptyset_i\tilde{\eth}_{2ij}^\top \\
* & -\tilde{\mathcal{S}}_1 & 0 & 0 \\
* & * & -\emptyset_i I & 0 \\
* & * & * & -\emptyset_i I
\end{bmatrix} < 0, \qquad (35)
$$

where

$$
\begin{aligned}
\widehat{\Xi}_{ij}(\bar{d}) &= \widehat{\Xi}_{01}(\bar{d}) + \widehat{\Xi}_{02}(\bar{d}),\\
\widehat{\Xi}_{01}(\bar{d}) &= \widehat{\chi}_1 + \widehat{\chi}_2 + \widehat{\chi}_3 + \widehat{\chi}_4 + \widehat{\Omega}_{3ij} + e_{10}^T \frac{-\alpha}{\hat{w}^2} I e_{10},\\
\widehat{\Xi}_{02}(\bar{d}) &= (\frac{\bar{h}_d}{\bar{h}} + \frac{\bar{d}^2}{\bar{h}^2}) Sym[\tilde{\mathcal{Y}}_1 \mathcal{X}_1 + \tilde{\mathcal{Y}}_2 \mathcal{X}_2]\\
&\quad - (\frac{\bar{h}_d}{\bar{h}^2} \mathcal{X}_1^\top \tilde{\mathcal{S}}_1 \mathcal{X}_1 + \frac{\bar{d}}{\bar{h}^2} [\mathcal{X}_2^\top \tilde{\mathcal{S}}_1 \mathcal{X}_2)],\\
\tilde{\tilde{\phi}} &= \frac{1}{\bar{h}^2} He[\tilde{\mathcal{Y}}_1 \mathcal{X}_1 + \tilde{\mathcal{Y}}_2 \mathcal{X}_2],\ \tilde{\mathcal{S}}_1 = diag\{\tilde{\mathcal{S}}_1, 3\tilde{\mathcal{S}}_1, 5\tilde{\mathcal{S}}_1\},\\
\widehat{\chi}_1 &= sym\{\alpha e_1 \tilde{\mathcal{P}} e_1^\top + e_1 \tilde{\mathcal{P}} e_5^\top\},\\
\widehat{\chi}_2 &= -\mathbf{h}(2(e_2 - e_4)^\top \tilde{\mathcal{S}}_2 e_4 + \bar{h} e_4^\top \tilde{\mathcal{S}}_3 e_4) + \bar{h} \mathcal{F}^\top \tilde{\mathcal{S}} \mathcal{F} + \hat{\Xi}_{02}(\bar{d}),\\
\widehat{\chi}_3 &= e_1^\top [\bar{h}\tilde{\mathcal{U}}_{11} + 2\tilde{\mathcal{U}}_{13}] e_1 + 2 e_1^\top [\bar{h}\tilde{\mathcal{U}}_{12} - \tilde{\mathcal{U}}_{13} + \tilde{\mathcal{U}}_{13}^\top] e_3\\
&\quad + e_3^\top [\bar{h}\tilde{\mathcal{U}}_{22} - \tilde{\mathcal{U}}_{23} + \tilde{\mathcal{U}}_{23}^\top] e_3,\\
\widehat{\chi}_4 &= \bar{h} e_5^\top \tilde{\mathcal{T}} e_5 + \widehat{\chi}_3,\\
\widehat{\Omega}_{3ij} &= -k_1 e_1^\top \tilde{\mathcal{W}} e_5 + 2k_1 e_1^\top A_i \tilde{\mathcal{W}} e_1 + k_1 e_1^\top B_i \mathbb{Y}_j e_4\\
&\quad - 2k_2 e_5^\top \tilde{\mathcal{W}}^\top e_5 + k_2 e_1^\top \tilde{\mathcal{W}} A^\top e_5 + k_2 e_4^\top B_i^\top \mathbb{Y}_j^\top e_5\\
&\quad - k_3 e_4^\top \tilde{\mathcal{W}}^\top e_5 + k_3 e_1^\top A_i^\top \tilde{\mathcal{W}} e_4 + 2k_3 e_4^\top B_i \mathbb{Y}_j e_4\\
&\quad + e_1^T k_1 \tilde{\mathcal{W}} E_i e_{10} + e_5^T k_2 \tilde{\mathcal{W}} E_i e_{10} + e_4^T k_3 \tilde{\mathcal{W}} E_i e_{10},\\
\tilde{\delta}_{1ij} &= [k_1 \mathcal{H}_{1j}\ 0\ 0\ k_3 \mathcal{H}_{1j}\ k_2 \mathcal{H}_{1j}\ 0_{1\times 5}],\\
\tilde{\delta}_{2ij} &= [0\ 0\ 0\ \mathcal{M}_{1j} \mathbb{Y}_j\ 0_{1\times 6}].
\end{aligned}
$$

Then the reachable set of system (14) are bounded $\epsilon(\mathcal{P})$ such that $\{x(t) \in \mathbb{R}^n \mid \|x(t)\| \le \hat{r}\}$ with $\hat{r} = \frac{1}{\sqrt{\lambda_{min}(\mathcal{P})}}$. Furthermore, under these conditions, the NFSDC gains $\mathcal{K}_j$ in (12) are achieved by $\mathcal{K}_j = \mathbb{Y}_j \mathbb{W}^{-1}$.

Proof. Following the same proof procedure as in Theorem 6.1 and define $\mathcal{W}_1 = k_1\mathbb{W}$, $\mathcal{W}_2 = k_2\mathbb{W}$, $\mathcal{W}_3 = k_3\mathbb{W}$, $\tilde{\mathcal{W}} = \mathbb{W}^{-1}$, $\mathbb{Y}_j = \mathcal{K}_j\mathbb{W}$, $\tilde{\mathcal{P}} = \tilde{\mathcal{W}}\mathcal{P}\tilde{\mathcal{W}}$, $\tilde{\mathcal{S}}_1 = \tilde{\mathcal{W}}\mathcal{S}_1\tilde{\mathcal{W}}$, $\tilde{\mathcal{S}}_2 = \tilde{\mathcal{W}}\mathcal{S}_2\tilde{\mathcal{W}}$, $\tilde{\mathcal{S}}_3 = \tilde{\mathcal{W}}\mathcal{S}_3\tilde{\mathcal{W}}$, $\tilde{\mathcal{U}}_{11} = \tilde{\mathcal{W}}\mathcal{U}_{11}\tilde{\mathcal{W}}$, $\tilde{\mathcal{U}}_{12} = \tilde{\mathcal{W}}\mathcal{U}_{12}\tilde{\mathcal{W}}$, $\tilde{\mathcal{U}}_{13} = \tilde{\mathcal{W}}\mathcal{U}_{13}\tilde{\mathcal{W}}$, $\tilde{\mathcal{U}}_{22} = \tilde{\mathcal{W}}\mathcal{U}_{22}\tilde{\mathcal{W}}$, $\tilde{\mathcal{U}}_{23} = \tilde{\mathcal{W}}\mathcal{U}_{23}\tilde{\mathcal{W}}$, $\tilde{\mathcal{T}} = \tilde{\mathcal{W}}\mathcal{T}\tilde{\mathcal{W}}$, $\tilde{\mathcal{Y}}_1 = \tilde{\mathcal{W}}\mathcal{Y}_1\tilde{\mathcal{W}}$, $\tilde{\mathcal{Y}}_2 = \tilde{\mathcal{W}}\mathcal{Y}_2\tilde{\mathcal{W}}$. Pre- and post-multiplying (16), (17), and (18) by $diag\{\underbrace{\tilde{\mathcal{W}}, \tilde{\mathcal{W}}, \tilde{\mathcal{W}}}_{9\ times}, I, \tilde{\mathcal{W}}, I, I\}$, we get (33), (34), and (35). This completes the proof. □

Remark 6.4. It is noteworthy that, in many industrial process, the dynamic behaviors are generally complex and nonlinear, and their real mathematical models are always difficult to obtain. How to design the non-fragile sampled-data control (NFSDC) for the PMSM model and analysis of the reachable set estimation has become one main focus of research. More particularly, some pioneering works have been discussed in sampled-data control for the PMSM model. In [22], bifurcation analysis and the problem of T-S fuzzy sampled-data stabilization of PMSM have been studied. Reliable fuzzy H_∞ control has been designed for the PMSM model against stochastic actuator faults in [4]. Nien-Tan fuzzy method has been proposed in [25] for wind energy conversion system via SDC. Recently in [27], fuzzy SDC has been studied for PMSM-based wind turbine system. The model considered in the present study is more practical than that proposed by [4,22,25,27] because they consider usual sampled-data control has been studied with a fuzzy system based on stability analysis via PMSM model, but in this paper, we consider a new reachable set estimation and bifurcation analysis with the combination of NFSDC in the considered PMSM model. Due to the many real-life application the combined study of bifurcation analysis and reachable set estimation for NFSDC effects on the PMSM model is more important. Inspired by the idea of [36] the composite slack variable inequality (CSVI) was applied in this paper, as a result, the CVSI technique has provided a tighter upper bound analysis for such LKFs, which can improve the stability performance with less conservative results rather than these of [26,38,39], which has been shown in comparison example section (Table 3) in the revised manuscript. Henceforth, the investigation procedure and framework model proposed in this study merit a lot of regard for filling such demand all the more successfully.

7. Numerical simulation:

In this part of the article, the whole dynamical differential model of PMSM is solved with the assistance of the Matlab LMI control toolbox. Additionally, the viability of the suggested approach and its superiority are validated at this point. Table 1 provides a definition of the numerical values of the system parameters that are utilized for simulations.

Table 1
Parameters of the PMSM.

Symbol	Value
L_d	15
L_q	11
R_1	0.9010
J	4.7×10^{-3}
ψ_r	1.8
β	0.0162
n_p	1

7.1. Simulation for PMSM model (1)

The obtained necessary conditions from the previous section, which demonstrate the RSE of the closed-loop system (14) are discussed in this part together with the dynamical behavior of the PMSM model (1) with a non-smooth-air-gap. The steps are provided in Algorithm1.

The specified scalars are chosen as $\bar{h} = 0.01$ and the parameter of α is chosen as $\alpha = 0.25$. The LMIs (33)–(35) in Theorem 6.3 can be solved using the aforementioned parameters together with $w(t) = 0.2+0.01rand$, $B_i = [1\ 1\ 0]^T$, $E_i = [0\ 0\ T_1]^T$, $(i = 1, 2, 3, 4)$, $\mathcal{H}_l = diag\{0.1, 0.1, 0.1\}$, $\mathcal{M}_l = diag\{0.5, 0.5, 0.5\}$, $W_1 = 1$, $W_2 = 12$, and the maximum upper bound of the sampling interval $\bar{h}$ is obtained as $\bar{h} = 0.01$. Additionally, the associated control gain matrices are computed as

$$\mathcal{K}_1 = [-6.4051\ \ -0.3120\ 2.2334],$$
$$\mathcal{K}_2 = [-4.4322\ 2.1133\ 1.1011],$$
$$\mathcal{K}_3 = [-5.4051\ \ -1.3120\ 2.2334],$$
$$\mathcal{K}_4 = [-3.4322\ 2.1133\ 1.1011].$$

To stabilize the closed-loop system (14), the estimated control gains are included in the suggested control input (13), and the state responses of PMSM with and without NFSDC-based PMSM are depicted in the figures. 7 and 8. From Fig. 7, the non-linear model (2) revealed the unpredictable behaviors of their states with respect to different operating parameters. Furthermore, Fig. 8 confirms that when using the NFSDC in (14), the PMSM model is effectively controlled even in the occurrence of small uncertainties in the controller. The bounding ellipsoid are shown in Fig. 9. Thus the effectiveness of the proposed method can be verified.

Algorithm 1: Stabilization analysis of the PMSM model (14)

Step 1: Set the PMSM model parameters A_i, B_i, and E_i uncertain parameters $\mathcal{H}_{1j}$, $\mathcal{M}_{1j}$ and define the symmetric matrices $\tilde{\mathcal{P}} > 0, \tilde{\mathcal{S}}_1 > 0, \tilde{\mathcal{S}}_2 > 0, \tilde{\mathcal{S}}_3 > 0, \tilde{\mathcal{T}} > 0, \tilde{\mathcal{Y}}_1 > 0, \tilde{\mathcal{Y}}_2 > 0, \tilde{\mathcal{U}} = [\tilde{\mathcal{U}}_{mn}]_{3\times 3} \geq 0$ with set the upper bound of sampling instants $h_k \in (0, \bar{h}]$.
Assure: Verify the feasibility of LMI.
Need: Find the control gain matrices.
Step 2: Use the sampling conditions and novel LKF techniques to construct the LMIs in Theorem 6.3
Step 3: Adjust the value of α and $\bar{h}$ to calculate whether the solution of LMI exists.
Step 4: Solve: (33)–(35) in Theorem 6.3 and check the feasibility of LMI using MATLAB control toolbox.
Step 5: If the feasible solution exists, stop the calculation and obtain the maximum value of $\bar{h}$ and the controller gains $\mathcal{K}_j$, else go to step 3 and increase or decrease the value of $\bar{h}$ and α.
Step 6: Stop.

Therefore, based on the described simulation, the uncertainties are also effectively estimated through the proposed NFSDC. Furthermore, to establish the effectiveness of the designed NFSDC, different sampling interval values, and its corresponding control gains are tabulated in Table 2.

8. Comparative example (Effectiveness of NFSDC scheme)

The effectiveness and superiority of the intended NFSDC are demonstrated in this paragraph by examining and resolving Rossler's system, [38]. Input terms and the dynamics of Rossler's system are described by

$$\begin{cases} \dot{x}_1(t) = -x_2(t) - x_3(t), \\ \dot{x}_2(t) = x_1(t) + \tau_2 x_2(t) \\ \dot{x}_3(t) = \tau_3 x_1(t) - (\tau_4 - x_1(t)x_3(t) + u(t)) \end{cases} \tag{36}$$

Table 2
Largest sampling interval $\bar{h}$ and the corresponding control gain matrices.

$\bar{h}$	Gain matrices
0.01	$\mathscr{K}_1 = [-6.4062 \ -0.5120 \ 2.4334]$ $\mathscr{K}_2 = [-4.4322 \ 2.1133 \ 1.1011]$ $\mathscr{K}_3 = [-5.4062 \ -1.5120 \ 1.4334]$ $\mathscr{K}_4 = [-2.4322 \ 1.6133 \ 2.1011]$
0.05	$\mathscr{K}_1 = [-6.4062 \ -0.5120 \ 2.4334]$ $\mathscr{K}_2 = [-4.4322 \ 2.1133 \ 1.1011]$ $\mathscr{K}_3 = [-5.4062 \ -1.5120 \ 1.4334]$ $\mathscr{K}_4 = [-2.4322 \ 1.6133 \ 2.1011]$
0.12	$\mathscr{K}_1 = [-12.1211 \ -1.1247 \ 2.7856]$ $\mathscr{K}_2 = [-5.4562 \ 3.8752 \ -1.0533]$ $\mathscr{K}_3 = [-6.9787 \ -4.0731 \ -2.9112]$ $\mathscr{K}_4 = [-3.1308 \ 5.0909 \ 1.3422]$

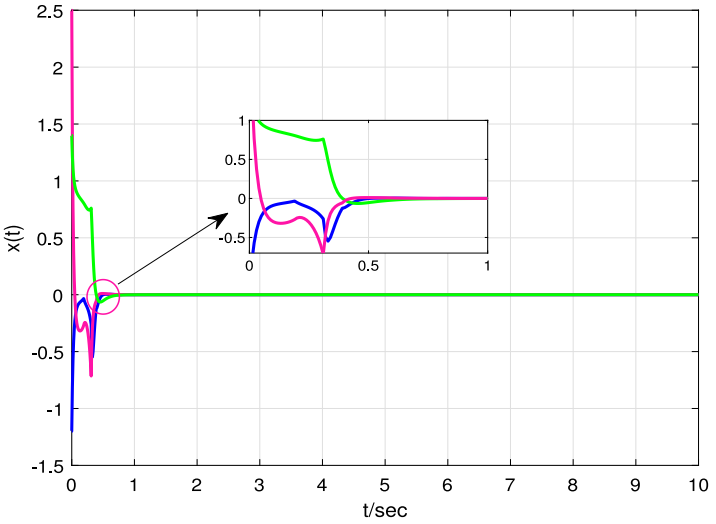

Fig. 7. State responses of the model (14).

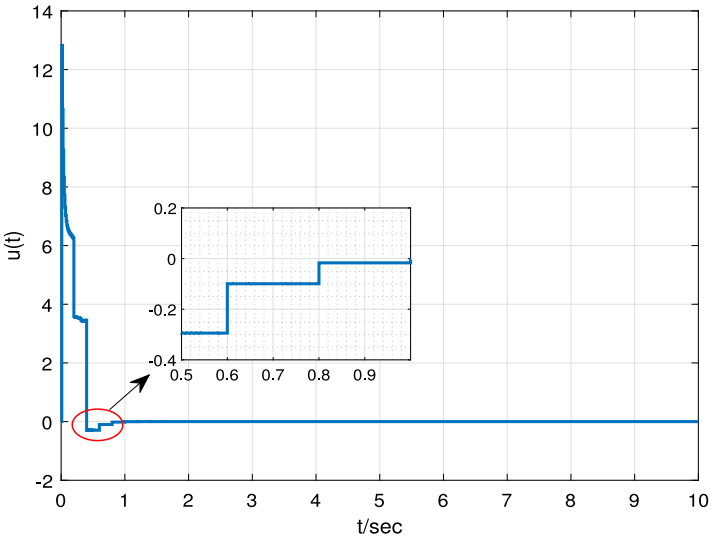

Fig. 8. Control response curve of the model (14).

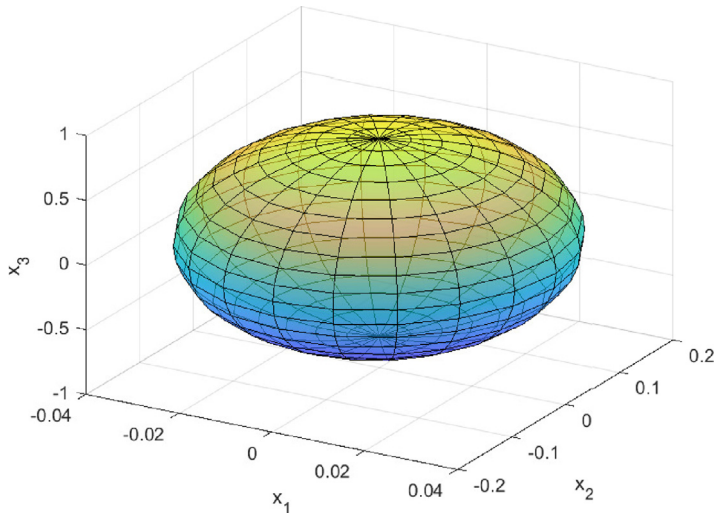

Fig. 9. Trajectories of the bounding ellipsoid.

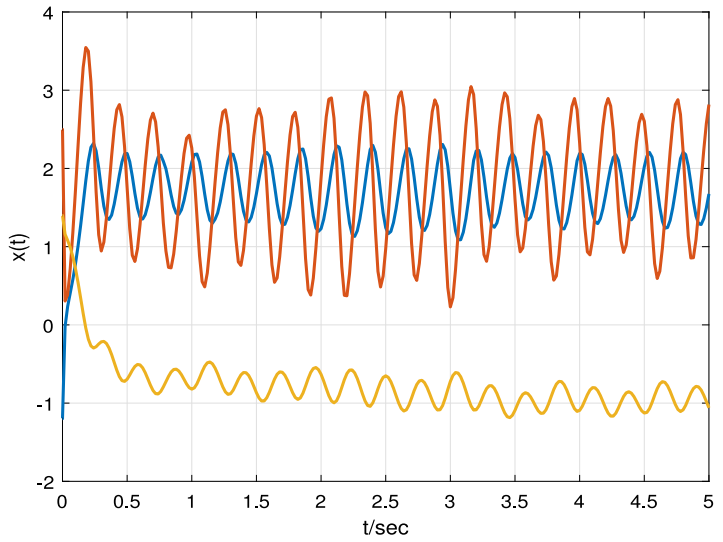

Fig. 10. Response curve of without control input model (36).

where τ_2, τ_3, and τ_4 are constants and $x_1(t)$, $x_2(t)$ and $x_3(t)$ are state variables. Control input is denoted by $u(t)$. The Rossler system with $x_1(t) \in [\tau_4 - \hat{\nu}, \tau_4 + \hat{\nu}]$ can be explain by the T-S fuzzy system with

$$A_1 = \begin{bmatrix} 0 & -1 & -1 \\ 1 & \tau_2 & 0 \\ \tau_3 & 0 & -\hat{\nu} \end{bmatrix}, \; A_2 = \begin{bmatrix} 0 & -1 & -1 \\ 1 & \tau_2 & 0 \\ \tau_3 & 0 & \hat{\nu} \end{bmatrix},$$

$$B_1 = B_2 = [0\ 0\ 1]^T,$$

and define the membership functions are $h_1(x_1(t)) = \frac{\tau_4 + \hat{\nu} - x_1(t)}{2\hat{\nu}}$ and $h_2(x_1(t)) = 1 - h_1(x_1(t))$. Assuming $\tau_2 = 0.3$, $\tau_3 = 0.5$, $\tau_4 = 5$, $\hat{\nu} = 10$, $\alpha = 0.1$, utilizing the values of the parameters listed and solving the LMIs in Theorem 6.3 with $E_i = 0$ (ie,) without disturbance and the maximum sampling interval bound can be calculated based on Theorem 6.3, which is listed in Table 3. As a result, we achieve the maximum sampling interval $\bar{h} = 0.1203$. Furthermore, Table 3 indicates that the comparison results of the conditions were derived with the largest sampling interval as in Theorem 6.3. Furthermore, the state trajectories of the system (36) with and without control input $u(t)$ are shown in Figs. 10 and 11 under the proposed controller scheme. The dynamic response of the control input is shown in Fig. 12. Finally, we conclude that non-linear systems (36) achieve the existence of the reachable set under the NFSDC scheme, and the conditions obtained yield better results than the existing results.

Table 3
Calculated maximum sampling interval $\bar{h}$.

Method	[38]	[26]	[39]	Theorem 6.3
$\bar{h}$	0.0959	0.1147	0.1165	0.1203

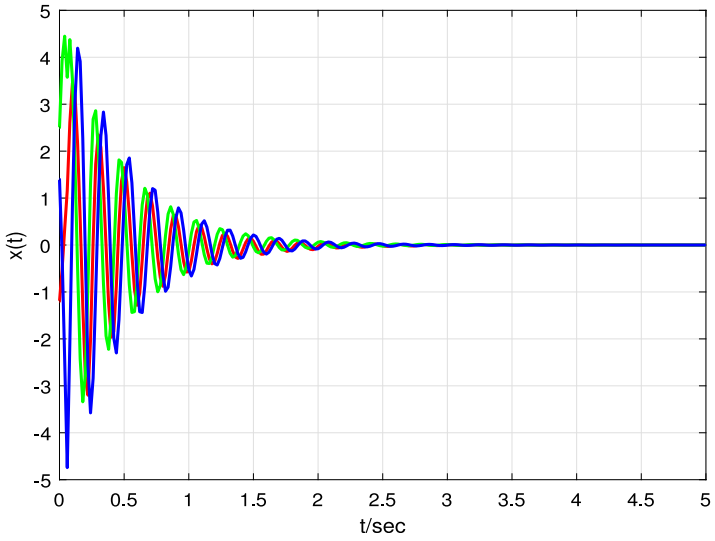

Fig. 11. State trajectories of the model (36).

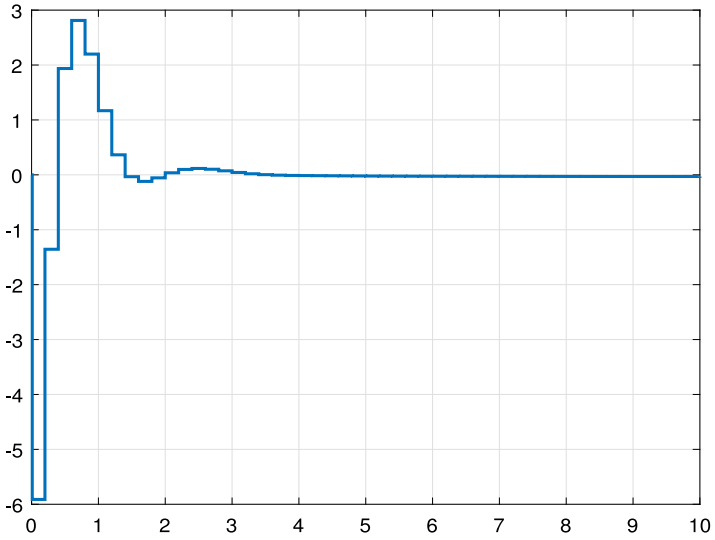

Fig. 12. Control response curve of the system (36).

9. Conclusion

In order to analyze the RSE synthesis of the PMSM system, NFSDC was used in this article. By applying the standard LKF, composite slack variable inequality, and other inequality techniques, the RSE of the closed-loop system has been attained and is bounded by an ellipsoid as tiny as possible, which has been obtained through LMIs. The NFSDC gains were then acquired by solving the LMIs. Furthermore, the suggested strategy reduces the conservatism of the current results. We will focus on the real-time RSE problem for PMSM models with unknown parameterizations in future studies, and the challenge of RSE under memory event-triggered control will be a challenging and practical topic of discussion to investigate.

CRediT authorship contribution statement

R. Vadivel: Conceptualization, Methodology, Writing – original draft. **Zeric Tabekoueng Njitacke:** Formal analysis, Validation, Software. **Lakshmanan Shanmugam:** Investigation, Software, Visualization. **P. Hammachukiattikul:** Methodology, Formal analysis. **Nallappan Gunasekaran:** Writing – review & editing, Supervision.

Declaration of competing interest

The authors declare that they have no known competing financial interests or personal relationships that could have appeared to influence the work reported in this paper.

Data availability

No data was used for the research described in the article.

References

[1] Robert B, Alin F, Goeldel C. Aperiodic and chaotic dynamics in hybrid step motor-new experimental results. In: ISIE 2001. 2001 IEEE international symposium on industrial electronics proceedings. Vol. 3. IEEE; 2001, p. 2136–41.
[2] Suto Z, Nagy I, Masada E. Avoiding chaotic processes in current control of AC drive. In: PESC 98 record. 29th Annual IEEE power electronics specialists conference. Vol. 1. IEEE; 1998, p. 255–61.
[3] Li Z, Park JB, Joo YH, Zhang B, Chen G. Bifurcations and chaos in a permanent-magnet synchronous motor. IEEE Trans Circuits Syst I 2002;49(3):383–7.
[4] Vadivel R, Joo YH. Reliable fuzzy H_∞ control for permanent magnet synchronous motor against stochastic actuator faults. IEEE Trans Syst Man Cybern Syst 2019;51(4):2232–45.
[5] Chen J, Chau K, Chan CC. Analysis of chaos in current-mode-controlled DC drive systems. IEEE Trans Ind Electron 2000;47(1):67–76.
[6] Chen J, Chau K, Chan C, Jiang Q. Subharmonics and chaos in switched reluctance motor drives. IEEE Trans Energy Convers 2002;17(1):73–8.
[7] Gao Y, Chau K. Hopf bifurcation and chaos in synchronous reluctance motor drives. IEEE Trans Energy Convers 2004;19(2):296–302.
[8] Hemati N. Strange attractors in brushless DC motors. IEEE Trans Circuits Syst I 1994;41(1):40–5.
[9] Jing Z, Yu C, Chen G. Complex dynamics in a permanent-magnet synchronous motor model. Chaos Solitons Fractals 2004;22(4):831–48.
[10] Zhang S, Wang C, Zhang H, Ma P, Li X. Dynamic analysis and bursting oscillation control of fractional-order permanent magnet synchronous motor system. Chaos Solitons Fractals 2022;156:111809.
[11] Cheukem A, Kemnang Tsafack AS, Takougang Kingni S, André CC, Mboupda Pone JR. Permanent magnet synchronous motor: chaos control using single controller, synchronization and circuit implementation. SN Appl Sci 2020;2(3):1–11.
[12] Singh JP, Roy BK, Kuznetsov NV. Multistability and hidden attractors in the dynamics of permanent magnet synchronous motor. Int J Bifurcation Chaos 2019;29(04):1950056.
[13] Mao D, Ma Y. Finite-time mixed H_∞ and passivity analysis for Takagi–Sugeno fuzzy system with time-varying delays and actuator faults. Commun Nonlinear Sci Numer Simul 2023;116:106770.
[14] Takagi T, Sugeno M. Fuzzy identification of systems and its applications to modeling and control. IEEE Trans Syst Man Cybern 1985;(1):116–32.
[15] Shi K, Wang J, Zhong S, Tang Y, Cheng J. Non-fragile memory filtering of T–S fuzzy delayed neural networks based on switched fuzzy sampled-data control. Fuzzy Sets and Systems 2020;394:40–64.
[16] Shi K, Wang J, Tang Y, Zhong S. Reliable asynchronous sampled-data filtering of T–S fuzzy uncertain delayed neural networks with stochastic switched topologies. Fuzzy Sets and Systems 2020;381:1–25.
[17] Cheng J, Zhang D, Qi W, Cao J, Shi K. Finite-time stabilization of T–S fuzzy semi-Markov switching systems: A coupling memory sampled-data control approach. J Franklin Inst B 2020;357(16):11265–80.
[18] Mani P, Rajan R, Shanmugam L, Joo YH. Adaptive fractional fuzzy integral sliding mode control for PMSM model. IEEE Trans Fuzzy Syst 2018;27(8):1674–86.
[19] Zhang D, Cai W, Xie L, Wang Q-G. Nonfragile distributed filtering for T–S fuzzy systems in sensor networks. IEEE Trans Fuzzy Syst 2014;23(5):1883–90.
[20] Cai X, Wang J, Zhong S, Shi K, Tang Y. Fuzzy quantized sampled-data control for extended dissipative analysis of T–S fuzzy system and its application to WPGSs. J Franklin Inst B 2021;358(2):1350–75.
[21] Vadivel R, Joo YH. Finite-time sampled-data fuzzy control for a non-linear system using passivity and passification approaches and its application. IET Control Theory Appl 2020;14(8):1033–45.
[22] Vadivel R, Srinivasan S, Wu Y, Gunasekaran N. Study on bifurcation analysis and Takagi–Sugeno fuzzy sampled-data stabilization of permanent magnet synchronous motor systems. Math Methods Appl Sci.
[23] Ji H, Cui B, Liu X. Networked sampled-data control of distributed parameter systems via distributed sensor networks. Commun Nonlinear Sci Numer Simul 2021;98:105773.
[24] Fan Y, Huang X, Wang Z, Xia J, Shen H. Resilient sampled-data control for stabilization of T-S fuzzy systems via interval-dependent function method: Handling DoS attacks. IEEE Trans Fuzzy Syst 2022.
[25] Gunasekaran N, Joo YH. Nie–Tan fuzzy method of fault-tolerant wind energy conversion systems via sampled-data control. IET Control Theory Appl 2020;14(11):1516–23.
[26] Zhang R, Zeng D, Park JH, Liu Y, Zhong S. A new approach to stabilization of chaotic systems with nonfragile fuzzy proportional retarded sampled-data control. IEEE Trans Cybern 2018;49(9):3218–29.
[27] Shanmugam L, Joo YH. Stabilization of permanent magnet synchronous generator-based wind turbine system via fuzzy-based sampled-data control approach. Inform Sci 2021;559:270–85.
[28] Yu Y, Shen Y, Liu Y. Sampled-data based output tracking H_∞ control for PMSM servo system. In: 2017 Chinese automation congress. IEEE; 2017, p. 5521–5.
[29] Al Tahir A, El Magri A, Ahmed-Ali T, El Fadili A, Giri F. Sampled-data nonlinear observer design for sensorless synchronous PMSM. IFAC-PapersOnLine 2015;48(11):327–32.
[30] Feng Z, Zheng WX, Wu L. Reachable set estimation of T–S fuzzy systems with time-varying delay. IEEE Trans Fuzzy Syst 2016;25(4):878–91.
[31] Fridman E, Shaked U. On reachable sets for linear systems with delay and bounded peak inputs. Automatica 2003;39(11):2005–10.

[32] Wang L, Xia J, Chen G, Park JH, Shen H. Reachable set estimation and aperiodic sampled-data controller design for Markovian jump systems. Internat J Robust Nonlinear Control 2021;31(17):8442–62.
[33] Zhong Z, Zhu Y, Ahn CK. Reachable set estimation for Takagi-Sugeno fuzzy systems against unknown output delays with application to tracking control of AUVs. ISA Trans 2018;78:31–8.
[34] Lin W-J, He Y, Wu M, Liu Q. Reachable set estimation for Markovian jump neural networks with time-varying delay. Neural Netw 2018;108:527–32.
[35] Liu G, Xu S, Liu W, Chu Y, Zhang Z. Reachable set estimation and controller design for discrete-time singularly perturbed systems with time-varying delay. Internat J Robust Nonlinear Control 2021;31(15):7207–18.
[36] Tian Y, Wang Z. Composite slack-matrix-based integral inequality and its application to stability analysis of time-delay systems. Appl Math Lett 2021;120:107252.
[37] Liu P-L. Improved delay-dependent stability of neutral type neural networks with distributed delays. ISA Trans 2013;52(6):717–24.
[38] Liu Y, Park JH, Guo B-Z, Shu Y. Further results on stabilization of chaotic systems based on fuzzy memory sampled-data control. IEEE Trans Fuzzy Syst 2017;26(2):1040–5.
[39] Hua C, Wu S, Guan X. Stabilization of T-S fuzzy system with time delay under sampled-data control using a new looped-functional. IEEE Trans Fuzzy Syst 2019;28(2):400–7.